



# In vitro metabolism of cathinone positional isomers: does sex matter?

Peng Che<sup>1,2</sup> · J. Tyler Davidson<sup>3</sup> · Kristina Still<sup>1,2</sup> · Jeroen Kool<sup>1,2</sup> · Isabelle Kohler<sup>1,2,4</sup>

Received: 26 April 2023 / Revised: 16 June 2023 / Accepted: 19 June 2023 / Published online: 15 July 2023  
© The Author(s) 2023

## Abstract

Synthetic cathinones, one of the most prevalent categories of new psychoactive substances, have been posing a serious threat to public health. Methylmethcathinones (MMCs), notably 3-MMC, have seen an alarming increase in their use in the last decade. The metabolism and toxicology of a large majority of synthetic cathinones, including 3-MMC and 2-MMC, remain unknown. Traditionally, male-derived liver materials have been used as in vitro metabolic incubations to investigate the metabolism of xenobiotics, including MMCs. Therefore, little is known about the metabolism in female-derived in vitro models and the potential sex-specific differences in biotransformation. In this study, the metabolism of 2-MMC, 3-MMC, and 4-MMC was investigated using female rat and human liver microsomal incubations, as well as male rat and human liver microsomal incubations. A total of 25 phase I metabolites of MMCs were detected and tentatively identified using liquid chromatography-tandem mass spectrometry (LC-MS/MS). Seven sex-specific metabolites were detected exclusively using pooled male rat liver microsomal incubations. In addition, the metabolites generated from the sex-dependent in vitro metabolic incubations that were present in both male and female rat liver microsomal incubations showed differences in relative abundance. Yet, neither sex-specific metabolites nor significant differences in relative abundance were observed from pooled human liver microsomal incubations. This is the first study to report the phase I metabolic pathways of MMCs using in vitro metabolic incubations for both male and female liver microsomes, and the relative abundance of the metabolites observed from each sex.

**Keywords** Synthetic cathinones · Positional isomers · In vitro metabolism · Sex-specific differences · Methylmethcathinones

## Introduction

New psychoactive substances (NPS), also referred to as designer drugs or “legal highs,” are defined as new narcotic/psychotropic drugs which are not controlled by the United Nations’ 1961 Narcotic Drugs and the 1971 Psychotropic

Substances Conventions. These synthetic alternatives to conventional illicit drugs can pose a significant threat to the public health [1, 2]. Indeed, the NPS market is dynamic, with multiple new substances emerging each year, leading to challenges in monitoring and controlling these substances. Besides, the little information available on their pharmacology and toxicology can result in harmful consequences [2, 3]. Since most NPS are typically not controlled, they are easily available online or on the street market under the names “research chemicals”, “bath salts”, or “plant food” [4–6]. In the last decades, the category of synthetic cathinones (SCs) has seen a rise in its popularity worldwide, particularly among the young population [5, 6]. In 2020, SCs accounted for 65% of NPS material seized in Europe. Moreover, they currently represent the second largest category of NPS in terms of number of substances [7, 8]. SCs show cocaine- and amphetamine-like effects. Desired effects include increased energy, empathy, openness, and increased libido [9]. Both cardiovascular and neurological side effects have been reported, which are related to a decrease in the reuptake of norepinephrine, dopamine, and serotonin [10],

✉ Isabelle Kohler  
i.kohler@vu.nl

<sup>1</sup> Division of Bioanalytical Chemistry, Department of Chemistry and Pharmaceutical Sciences, Amsterdam Institute of Molecular and Life Sciences (AIMMS), Vrije Universiteit Amsterdam, De Boelelaan 1085, 1081 HV Amsterdam, The Netherlands

<sup>2</sup> Center for Analytical Sciences Amsterdam (CASA), Amsterdam, The Netherlands

<sup>3</sup> Department of Forensic Science, Sam Houston State University, Huntsville, TX, USA

<sup>4</sup> Co van Ledden Hulsebosch Center (CLHC), Amsterdam Center for Forensic Science and Medicine, Amsterdam, The Netherlands

as well as an increased release of dopamine [11]. Among all SCs, methylmethcathinone (MMC) isomers have been very popular among drug users, especially 3-methylmethcathinone (3-MMC) and 4-methylmethcathinone (4-MMC) [12, 13].

4-MMC, also known as mephedrone, has similar pharmacological effects to 3,4-methylenedioxymethamphetamine (MDMA, ecstasy) but with stronger craving feelings [14]. Due to its rapid increase in consumption and associated toxicology, 4-MMC has been banned in most European countries since 2010 [15]. As a consequence, its structural derivatives, such as 3-MMC, rapidly emerged on the drug market to replace 4-MMC [16, 17]. Due to an increase in the adverse events reports for 3-MMC worldwide and especially in Europe, the substance has been recently placed on the list of NPS under intensive monitoring by the European Monitoring Centre for Drugs and Drug Addiction (EMCDDA) [12]. The Netherlands currently represents an active player in NPS production, sale, and distribution within Europe, with 18 kg of 3-MMC powder shipped to European countries in 2020 [12]. The Dutch Poisons Information Center (DPIC) had seen a significant rise in the number of 3-MMC intoxication cases in 2020 and 2021 [13]. Due to multiple adverse events reported in the Netherlands and a growing concern, 3-MMC has been placed on the List II of the Opium Act in October 2021. As of now, more than 20 European countries have reported that 3-MMC is subject to restrictive measures at their national level [12]. Although 2-methylmethcathinone (2-MMC) has been less popular than other SCs, the ban of 3-MMC may shift the attention of drug users to other currently legal alternatives, such as 2-MMC.

The metabolism and toxicology of 4-MMC have already been investigated [18–24]. However, the metabolism of its positional isomers 3-MMC and 2-MMC remains mostly unknown. Moreover, little is known about the possible activity and/or toxicity of their metabolites. Information on drug metabolism is essential for forensic and toxicological purposes [25]. Due to ethical considerations, the investigation of NPS biotransformation is generally carried out using *in vitro* models, such as rat liver microsomes [26], human liver microsomes [21, 25, 27, 28], human hepatocytes [29], human S9 fractions [25, 30], or HepaRG cells [30]. These biological materials for *in vitro* incubations all contain drug-metabolizing enzymes, such as the cytochrome P450s (CYPs) complex.

Traditionally, metabolism studies are performed using male-derived materials. Indeed, women/females have been often excluded from (pre-)clinical trials and (pre-)clinical research investigating the effects and metabolism of drugs, regardless of the fact that substantial differences in pharmacokinetics and pharmacodynamics of drugs may exist between males and females, depending on the substance [31–33]. Until now, literature regarding potential sex-specific effects and metabolism of NPS in the organism remains very limited [34], even though sex-specific differences in pharmacokinetics and

pharmacodynamics have been demonstrated for traditional recreational drugs, such as cannabinoids, cocaine, and morphine [35–37]. To the best of our knowledge, no study has investigated the effects of sex on the *in vitro* metabolism of SCs.

The objectives of this study are to identify the metabolites of MMCs using *in vitro* metabolic incubations and investigate potential sex-specific differences in MMCs biotransformation. The metabolites produced in *in vitro* models were analyzed and identified using liquid chromatography-tandem mass spectrometry (LC-MS/MS). As a confirmatory analysis, ultra-high pressure liquid chromatography combined with high-resolution mass spectrometry (UHPLC-HRMS) was used to further decipher metabolites that were co-eluting using conventional LC-MS/MS analysis. The identification of MMCs metabolites opens new avenues in clinical and forensic toxicology, by providing a better understanding of SC metabolism and helping with the interpretation of general unknown screening data. Moreover, the results highlight the importance of investigating sex-specific differences in NPS metabolism and risk assessment for clinical and forensic purposes.

## Material and methods

### Chemicals

Acetonitrile (LC-MS grade) and DMSO were purchased from Biosolve (Valkenswaard, The Netherlands). Formic acid (LC-MS grade) was obtained from Merck (Zwijndrecht, The Netherlands). Ultra-pure water was obtained from a Milli-Q Plus purification system (Millipore, Amsterdam, The Netherlands). Magnesium chloride, NADPH, glucose-6-phosphate, and glucose-6-phosphate dehydrogenase were purchased from Sigma (Zwijndrecht, The Netherlands). Pooled male rat (Sprague-Dawley) liver microsomes and pooled female rat (Sprague-Dawley) liver microsomes were obtained from Sigma-Aldrich (St. Louis, MO, USA). Pooled male human liver microsomes (Lot No. 2110108) and pooled female human liver microsomes (Lot No. 1210079) were obtained from XenoTech (Lenexa, Kansas City, KS, USA). 2-Methylmethcathinone (2-MMC) hydrochloride, 3-methylmethcathinone (3-MMC) hydrochloride, and 4-methylmethcathinone (4-MMC) hydrochloride standards were provided by the Amsterdam Dutch Police. All stock solutions were prepared in DMSO and stored at -80 °C until further use.

### Pooled liver microsomal incubations

In order to investigate the biotransformation of the MMC positional isomers, the phase I metabolism of 4-MMC, 3-MMC, and 2-MMC was simulated *in vitro* using pooled human and rat liver microsomes. Specifically, each positional isomer was

metabolized using pooled female human liver microsomes (pFHLM), pooled male human liver microsomes (pMHLM), pooled female rat liver microsomes (pFRLM), and pooled male rat liver microsomes (pMRLM). Each liver microsomal incubation was carried out in duplicate with a final volume of 100  $\mu\text{L}$ . The reaction mixture consisted of 2.5 mM  $\text{MgCl}_2$  in 0.1 M potassium phosphate buffer (pH 7.4) containing 10% pooled liver microsomes [38]. Each drug was used at a concentration of 100  $\mu\text{M}$  for all incubations. The incubations were initiated by addition of a NADPH regenerating system, resulting in a final concentration of 0.1 mM NADPH, 0.3 mM glucose-6-phosphate, and 0.4 U/mL glucose-6-phosphate dehydrogenase. The metabolic incubations took place at 37 °C for 60 min. The incubations were quenched with the addition of ice-cold acetonitrile, with a volume corresponding to twice the metabolic mixture volume, followed by centrifugation at  $13,760 \times g$  for 10 min at 4 °C. The supernatant was transferred to a new tube and evaporated with a vacuum-centrifuge until dryness. Prior to injection into the LC-UV or LC-MS/MS system, the dried residue was first dissolved with 40  $\mu\text{L}$  eluent B, followed by the addition of 60  $\mu\text{L}$  eluent A for reconstitution. Blank samples consisted of only DMSO without analyte; control samples were prepared without the addition of NADPH.

### Analysis of metabolic mixtures using liquid chromatography

The analysis of liver microsomal incubation mixtures was carried out using an Agilent 1260 Infinity II LC system (Waldbronn, Germany) equipped with an Agilent 1260 Infinity II Flexible Pump (G7104C), an Agilent 1260 Infinity II Variable Wavelength Detector (G7114A), an Agilent 1260 Infinity II Multicolumn Thermostat (G7116A), and an Agilent 1260 Infinity II Multisampler (G7167AA). The separation was carried out using an XBridge  $\text{C}_{18}$  column (4.6 mm  $\times$  100 mm, 3.5  $\mu\text{m}$  particle size). The column and autosampler temperatures were set as 30 °C and 4 °C, respectively. The injection volume was 20  $\mu\text{L}$ . The mobile phase was composed of water-acetonitrile-formic acid (97.9:2:0.1, v/v/v, eluent A) and acetonitrile-water-formic acid (97.9:2:0.1, v/v/v, eluent B). The separation gradient was the following: eluent B at 1% for 10 min, linear increase to 95% for 14 min, and isocratic step at 95% for 5 min. After each run, the column was re-equilibrated with the initial conditions for 5 min. The separation was performed at a flow rate of 0.6 mL/min. UV detection was performed at 254 nm and 280 nm.

### Metabolite identification using liquid chromatography-tandem mass spectrometry

Experiments for the identification of MMC metabolites were carried out using an Agilent 1260 Infinity II Analytical LC system connected to a maXis ultra-high resolution

time-of-flight mass spectrometer (UHR TOF/MS, Bruker Daltonics, Bremen, Germany) via an electrospray ionization (ESI) source. To achieve a stable electrospray ionization (ESI), a flow splitter was used between the LC system and MS system, allowing 10% of the flow to enter the ESI source. The ESI source was operated in positive ionization mode. The capillary voltage and end plate offset were set at 4500 V and 500 V, respectively. The pressure of the nebulizer gas (nitrogen) was set to 4 bar. The temperature and flow rate of the drying gas (nitrogen) were 220 °C and 4.0 L/min, respectively. The quadrupole was set in scan mode with a mass range from  $m/z$  50 to 400 at a spectral rate of 1 Hz. The AutoMS/MS mode was applied, where the five precursor ions from each cycle showing the highest intensity were selected for fragmentation. The product ions of MMCs were detected within a mass range of  $m/z$  50 to 400 in the TOF/MS. Additional MS and MS/MS parameters are detailed in Supplementary Table S1. For metabolite identification, raw acquisition data were processed using the DataAnalysis software package from Bruker and the Elemental Composition Calculator v1.0 (written by Jef Rozenski, 1999, <http://rna.rega.kuleuven.be/masspec/elcomp.htm>), using 5 mDa mass tolerance for precursor and product ions. The instrument was externally calibrated using a 5 mmol  $\text{L}^{-1}$  sodium formate clusters tune mix.

### Enhancing the confidence in metabolite identification using ultra-high pressure liquid chromatography-tandem mass spectrometry

In order to enhance the confidence in metabolite identification and explain the presence of controversial product ions in the MS/MS spectrum for some metabolites due to co-eluting compounds, the metabolic mixtures of cathinone positional isomers were also analyzed using an Agilent 1290 Infinity II Analytical UHPLC system (Waldbronn, Germany) connected to a SCIEX ZenoTOF 7600 time-of-flight mass spectrometer (SCIEX, Singapore). The UHPLC system was equipped with an Agilent 1290 Infinity II High Speed Pump (G7120A), an Agilent 1290 Infinity II Multicolumn Thermostat (G7116B), and an Agilent 1290 Infinity II Vialsampler (G7129B). The separation was carried out using a Phenomenex Luna Omega  $\text{C}_{18}$  column (2.1  $\times$  100 mm, 1.6  $\mu\text{m}$  particle size) protected by a Phenomenex  $\text{C}_{18}$  guard column. The column and autosampler temperatures were set as 35 °C and 4 °C, respectively. The injection volume was 10  $\mu\text{L}$ . The mobile phase was composed of water-formic acid (99.9:0.1, v/v, eluent A) and acetonitrile-formic acid (99.9:0.1, v/v, eluent B). The separation gradient was the following: 0–2 min 2% eluent B, 3–6 min linear increase to 10% eluent B, 6–7 min isocratic step at 10% eluent B, 7–11 min linear increase to 10% eluent B, 11–12 min isocratic step at 20% eluent B, 12–14 min a steep increase to 95% eluent B, 14–15 min isocratic at 95% eluent B, 15–16 min return to initial conditions

of 2% eluent B and equilibration for 1 min. The separation was performed at a flow rate of 0.6 mL/min.

The ESI source was operated in positive ionization mode and parameters were set as the following: spray voltage, 5.5 kV; source temperature, 500 °C; nebulizer gas pressure, 45 psi; drying gas pressure, 45 psi; curtain gas pressure, 30 psi; and CAD gas pressure, 7 psi. Additional conditions are detailed in Supplementary Table S2. Raw acquisition data were processed using the SciexOS software from SCIEX and the Elemental Composition Calculator v1.0 (written by Jef Rozenski, 1999, <http://ma.rega.kuleuven.be/masspec/elcomp.htm>), using 5 mDa mass tolerance for precursor and product ions.

## Results and discussion

### MS/MS fragmentation of cathinone positional isomers

MMCs were mostly detected as the  $[M + H]^+$  protonated precursor (theoretical  $m/z$  178.1226). Figure 1 shows the

product ion mass spectra observed for 2-MMC, 3-MMC, and 4-MMC.

The product ion mass spectra for MMC isomers revealed abundant *N*-containing product ions, such as the product ions at  $m/z$  160.1115 ( $C_{11}H_{14}N^+$ ) and  $m/z$  145.0886 ( $C_{10}H_{11}N^+$ ). The dominant loss of  $H_2O$  from the protonated precursor is a common fragmentation behavior for *N*-alkylated synthetic cathinones [39, 40]. In comparison, most other *N*-containing stimulants usually tend to lose the amine group (i.e.,  $\Delta = 31$  Da) at the beginning of the fragmentation process [20, 21], particularly tertiary amine synthetic cathinones [41]. However, the MMCs favored the loss of  $H_2O$  followed by the loss of a methyl radical (i.e.,  $\bullet CH_3$ ,  $\Delta = 15$  Da). This same fragmentation behavior was observed for most of the metabolites, since they share the same structural backbone. In theory, the loss of radicals from even-electron species is unfavoured under collision-induced dissociation (CID) conditions; however, this phenomenon has been observed for synthetic cathinones under CID conditions by several research groups [20, 39, 42]. For example, Pozo et al. observed a similar fragmentation pattern for

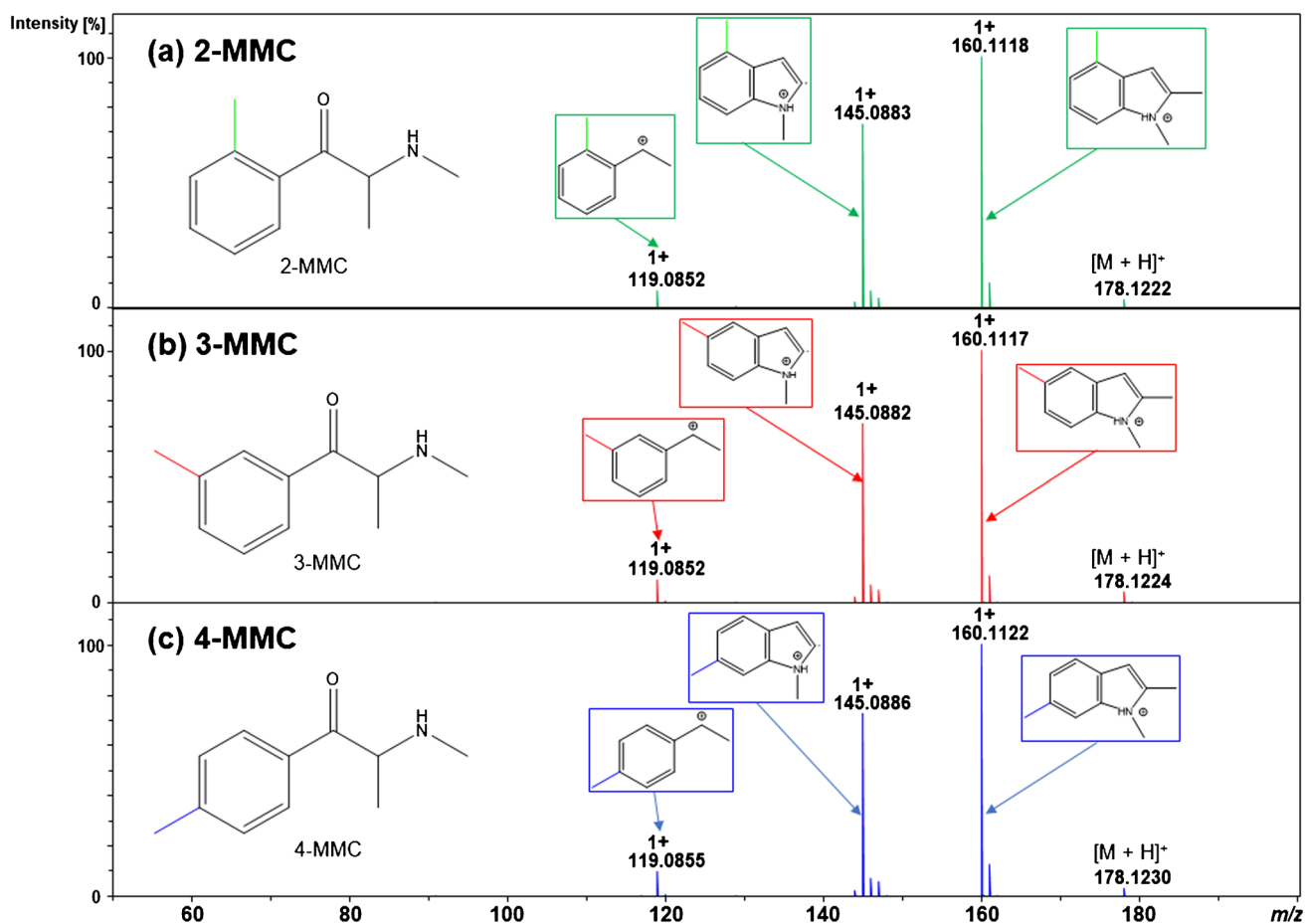


**Fig. 1** MS/MS spectra observed for 2-MMC (a, RT 16.4 min), 3-MMC (b, RT 16.5 min), and 4-MMC (c, RT 16.5 min) using a collision energy of 17.0 eV and indicating the proposed structures of the obtained product ions. Abbreviations: MMC, methylmethcathinone

4-MMC and demonstrated that an indole group was formed within 4-MMC due to an in-source intramolecular rearrangement occurring prior to fragmentation in the collision cell [20]. Besides this specific feature, the multiple protonation sites available on MMCs and their metabolites gave rise to diverse and competitive fragmentation patterns, making the interpretation of the MS/MS product ion mass spectra and elucidation of metabolite structures rather challenging, as discussed in the next sections.

### Metabolic profiling of cathinone positional isomers using in vitro metabolic incubations

Since rat liver microsomes and human liver microsomes share similarities in many CYP isoforms, the metabolites of the MMC positional isomers 2-MMC, 3-MMC, and 4-MMC identified in all in vitro metabolic incubations were expected to undergo similar modifications. The metabolism of 4-MMC, for instance, has been well investigated using different in vitro approaches [21, 24]. Most of the phase I metabolites of 4-MMC reported in previous studies were generated by four major metabolic biotransformation routes, namely (i) oxidative *N*-demethylation, (ii) oxidation of the 4-methyl group, (iii) omega-oxidation at the C-3' position, and (iv) carbonyl reduction, and via a combination of these reactions in the case of secondary metabolites [23]. However, for 2-MMC and 3-MMC, there is no information available in the literature related to their metabolism. The in vitro metabolism of 2-MMC and 3-MMC was therefore investigated.

### Identification of phase I metabolites of 2-methylmethcathinone

For each MMC positional isomer studied (i.e., 2-MMC, 3-MMC and 4-MMC), the fragmentation pattern was first investigated. This information subsequently enabled the tentative structural elucidation of their phase I metabolites. The phase I metabolites of 2-MMC, 3-MMC and 4-MMC identified are listed in Table 1.

**M1** This metabolite was only detected in pMRLM incubations, leading to a protonated precursor ion at  $m/z$  178.0878 ( $C_{10}H_{12}NO_2^+$ ). The empirical formula of the protonated precursor ion was derived based on the accurate mass measurement (see Table 1). The **M1** metabolite was formed from a combination of three metabolic reactions, namely, *N*-demethylation, *N*-oxidation, or omega-oxidation at the C-3' position, followed by dehydrogenation. The abundant diagnostic iminium ions at  $m/z$  86.0235 ( $C_3H_4NO_2^+$ ) and  $m/z$  58.0294 ( $C_2H_4NO^+$ ) indicate that an *N*-demethylation occurred and a carbonyl group was introduced to the

aliphatic chain. Yet, the MS/MS product ion mass spectrum of this metabolite is not sufficient to inform about the exact location where the carbonyl was introduced in the aliphatic chain, which needs further investigation. Additional ions that support this structural modification include product ions at  $m/z$  142.0649 ( $C_{10}H_8N^+$ ),  $m/z$  119.0489 ( $C_8H_7O^+$ ), and  $m/z$  91.0540 ( $C_7H_7^+$ ). The product ion mass spectra of many synthetic cathinones contain a tropylium ion at nominal  $m/z$  91, particularly for synthetic cathinones with at least four carbon alkyl chains [43], although in this case the presence of the methyl substitution to the aromatic ring leads to the formation of the methyl-substituted benzoylium ion (i.e.,  $m/z$  119.0489) and the tropylium ion through the loss of CO (i.e.,  $\Delta = 28$  Da). Interestingly, some artifact ions were also observed in the product ion mass spectrum, such as the abundant ions at  $m/z$  160.1118 ( $C_{11}H_{14}N^+$ ) and  $m/z$  145.0890 ( $C_{10}H_{11}N^+$ ), which could not have formed from **M1** given their elemental compositions and the accurate mass measurements acquired with the high-resolution mass analyzer (TOF/MS) instrument used in this study. Strikingly, the results obtained with UHPLC-MS/MS analysis revealed a lack of product ions at  $m/z$  160.1118 ( $C_{11}H_{14}N^+$ ) and  $m/z$  145.0890 ( $C_{10}H_{11}N^+$ ), which suggests that an interference co-eluted with **M1** under conventional LC separation conditions but was resolved using UHPLC conditions.

**M2–5** These four metabolites were all detected in pooled female and male rat liver microsomal (pRLM) incubations, but **M2–M4** were not found in female and male human liver microsomal (pHLM) incubations, with a protonated precursor ion at  $m/z$  194.1170 ( $C_{11}H_{16}NO_2^+$ ). This accurate mass measurement indicates that these metabolites show one additional oxygen atom compared to the parent compound 2-MMC ( $\Delta = 16$  Da). Since 2-MMC contains multiple potential hydroxylation sites, their respective MS/MS spectra were investigated to propose the most feasible oxidation site for each metabolite. **M2**, **M3**, and **M4** all generated the diagnostic product ion at nominal  $m/z$  135 corresponding to the hydroxylated methylbenzoylium ion ( $C_8H_7O_2^+$ ). In addition, only a single loss of  $H_2O$  was observed from their respective MS/MS product ion mass spectra, which also supports that one oxygen atom was introduced to an undetermined aromatic position. Additional support for the presence of hydroxylation on the aromatic ring includes the presence of product ions at nominal  $m/z$  161,  $m/z$  145, and  $m/z$  119. The product ion at nominal  $m/z$  161 ( $C_{10}H_{11}NO^+$ ) is formed through the loss of a methyl radical from the primary product ion at nominal  $m/z$  176 ( $C_{11}H_{14}NO^+$ ), which is formed through the loss of  $H_2O$  from the protonated precursor ion for **M2–M4**. The methyl radical (i.e.,  $\bullet CH_3$ ) can be lost from either the amine or aliphatic chain [20], which contributes to the abundance of this fragmentation pathway. The loss of the amine moiety from the primary product ion

**Table 1** Phase I metabolites of MMC positional isomers detected in liver microsomal incubations using LC-MS/MS

MMC positional isomers	Metabolites	RT (min)	In vitro models	Accurate <i>m/z</i> (measured)	Exact mass [M + H] <sup>+</sup>	Chemical formula	Modification(s)	Major product ions (abundance, %)	Error (ppm)*
2-MMC	M1	21.1	pMRLM	178.0878	178.0868	C <sub>10</sub> H <sub>12</sub> NO <sub>2</sub>	Aliphatic hydroxylation or <i>N</i> -oxidation; <i>N</i> -demethylation; dehydrogenation	160 (100%), 86 (55%), 119 (57%)	5.6
	M2	11.5	pMRLM; pFRLM	194.1191	194.1181	C <sub>11</sub> H <sub>16</sub> NO <sub>2</sub>	Aromatic hydroxylation	176 (100%), 119 (60%), 161 (30%)	5.2
	M3	14.3	pMRLM; pFRLM	194.1191	194.1181	C <sub>11</sub> H <sub>16</sub> NO <sub>2</sub>	Aromatic hydroxylation	176 (100%), 119 (92%), 145 (26%)	5.2
	M4	14.8	pMRLM; pFRLM	194.1191	194.1181	C <sub>11</sub> H <sub>16</sub> NO <sub>2</sub>	Aromatic hydroxylation	176 (100%), 161 (60%), 119 (11%)	5.2
	M5	17.4	pMRLM; pFRLM; pMHLM; pMHLM	194.1189	194.1181	C <sub>11</sub> H <sub>16</sub> NO <sub>2</sub>	Aliphatic hydroxylation or <i>N</i> -oxidation	119 (100%), 176 (4%), 74 (2%)	4.1
	M6	16.2	pMRLM; pFRLM; pMHLM; pMHLM	164.1085	164.1075	C <sub>10</sub> H <sub>14</sub> NO	<i>N</i> -demethylation	146 (100%), 131 (62%), 119 (14%)	6.1
3-MMC	M7	21.4	pMRLM	178.0862	178.0868	C <sub>10</sub> H <sub>12</sub> NO <sub>2</sub>	Aliphatic hydroxylation or <i>N</i> -oxidation; <i>N</i> -demethylation; dehydrogenation	160 (100%), 145 (72%), 86 (56%)	-3.4
	M8	8.7	pMRLM; pFRLM; pMHLM; pMHLM	194.1175	194.1181	C <sub>11</sub> H <sub>16</sub> NO <sub>2</sub>	Aliphatic hydroxylation	146 (100%), 158 (64%), 131 (10%)	-3.1
	M9	15.2	pMRLM; pFRLM;	194.1175	194.1181	C <sub>11</sub> H <sub>16</sub> NO <sub>2</sub>	Aromatic hydroxylation	176 (100%), 134 (86%), 161 (64%)	-3.1
	M10	17.6	pMRLM; pFRLM; pMHLM; pMHLM	194.1176	194.1181	C <sub>11</sub> H <sub>16</sub> NO <sub>2</sub>	Aliphatic hydroxylation or <i>N</i> -oxidation	119 (100%), 161 (8%), 91 (5%)	-2.6
	M11	15.6	pMRLM; pFRLM; pMHLM; pMHLM	164.1070	164.1075	C <sub>10</sub> H <sub>14</sub> NO	<i>N</i> -Demethylation	146 (100%), 131 (58%), 119 (14%)	-3.0
	M12	15.0	pMRLM; pFRLM	210.1124	210.1130	C <sub>11</sub> H <sub>16</sub> NO <sub>3</sub>	Di-hydroxylation or hydroxylation with <i>N</i> -oxidation	135 (100%), 174 (5%), 161 (5%)	-2.9
	M 13	6.8	pMRLM; pFRLM	180.1019	180.1025	C <sub>10</sub> H <sub>14</sub> NO <sub>2</sub>	Aliphatic hydroxylation; <i>N</i> -demethylation	160 (100%), 145 (78%), 144 (76%)	-3.3

**Table 1** (continued)

MMC positional isomers	Metabolites	RT (min)	In vitro models	Accurate $m/z$ (measured)	Exact mass [M + H] <sup>+</sup>	Chemical formula	Modification(s)	Major product ions (abundance, %)	Error (ppm)*
	M 14	19.2	pMRLM	180.1018	180.1025	C <sub>10</sub> H <sub>14</sub> NO <sub>2</sub>	Aliphatic hydroxylation; <i>N</i> -demethylation	144 (100%), 162 (73%), 120 (61%)	-3.9
	M15	18.9	pMRLM; pFRLM	192.1021	192.1025	C <sub>11</sub> H <sub>14</sub> NO <sub>2</sub>	Aliphatic hydroxylation; dehydrogenation	146 (100%), 131 (20%), 119 (15%)	-2.1
	M16	16.0	pMRLM	166.1226	166.1231	C <sub>10</sub> H <sub>16</sub> NO	<i>N</i> -Demethylation; reduction	148 (100%), 131 (44%), 120 (13%)	-3.0
	M17	11.9	pMRLM; pFRLM	208.0968	208.0974	C <sub>11</sub> H <sub>14</sub> NO <sub>3</sub>	Carboxylation	146 (100%), 85 (64%), 172 (38%)	-2.9
4-MMC	M18	15.7	pMRLM	178.0862	178.0868	C <sub>10</sub> H <sub>12</sub> NO <sub>2</sub>	Aliphatic hydroxylation; <i>N</i> -demethylation; dehydrogenation	160 (100%), 145 (72%), 148 (14%)	-3.4
	M19	21.3	pMRLM	178.0866	178.0868	C <sub>10</sub> H <sub>12</sub> NO <sub>2</sub>	Aliphatic hydroxylation or <i>N</i> -oxidation; <i>N</i> -demethylation; dehydrogenation	160 (100%), 145 (61%), 86 (33%)	-1.1
	M20	6.5	pMRLM; pFRLM; pMHLM; pMHLM	194.1179	194.1181	C <sub>11</sub> H <sub>16</sub> NO <sub>2</sub>	Aliphatic hydroxylation	146 (100%), 158 (70%), 131 (10%)	-1.0
	M21	17.5	pMRLM; pFRLM; pMHLM; pMHLM	194.1180	194.1181	C <sub>11</sub> H <sub>16</sub> NO <sub>2</sub>	Aliphatic hydroxylation or <i>N</i> -oxidation	119 (100%), 161 (7%), 91 (4%)	-0.5
	M22	16.3	pMRLM; pFRLM; pMHLM; pMHLM	164.1073	164.1075	C <sub>10</sub> H <sub>14</sub> NO	<i>N</i> -Demethylation	146 (100%), 131 (51%), 119 (18%)	-1.2
	M23	14.5	pMRLM; pFRLM	210.1130	210.1130	C <sub>11</sub> H <sub>16</sub> NO <sub>3</sub>	Di-hydroxylation or hydroxylation with <i>N</i> -oxidation	135 (100%), 161 (6%), 174 (4%)	0.0
	M24	19.3	pMRLM	180.1025	180.1025	C <sub>10</sub> H <sub>14</sub> NO <sub>2</sub>	Aliphatic hydroxylation; <i>N</i> -demethylation	160 (100%), 145 (91%), 144 (44%)	0.0
	M25	16.1	pMRLM	166.1230	166.1231	C <sub>10</sub> H <sub>16</sub> NO	<i>N</i> -Demethylation; reduction	148 (100%), 131 (44%), 120 (13%)	-0.6

\*The error refers to the relative mass difference expressed in ppm between the measured accurate mass of the metabolites and their theoretical exact mass. Abbreviations: *MMC*, methylmethcathinone; *RT*, retention time; *pMRLM*, pooled male rat liver microsomes; *pFRLM*, pooled female rat liver microsomes; *pMHLM*, pooled male human liver microsomes; *pFHLM*, pooled female human liver microsomes

at nominal  $m/z$  176 leads to the formation of the product ion at nominal  $m/z$  145 ( $C_{10}H_9O^+$ ). Subsequent loss of ethyne (i.e.,  $C_2H_2$ ) results in the formation of the product ion at nominal  $m/z$  119 ( $C_8H_7O^+$ ), still containing the hydroxylated substitution. **M5** was also detected in all metabolic incubations. From the MS/MS product ion mass spectrum of **M5**, the presence of the methyl-substituted benzoylium ion at  $m/z$  119.0502 ( $C_8H_7O^+$ ) supports that the hydroxylation cannot have occurred on the aromatic ring. A typical single loss of  $H_2O$  with a nominal mass shift of 18 Da and a double loss of  $H_2O$  with a nominal mass shift of 36 Da were observed. Yet, the MS/MS product ion mass spectrum of **M5** is not sufficient to reveal the exact location where oxygen was exactly introduced in the aliphatic chain, which also needs further investigation. Pedersen et al. report a similar issue when elucidating the structure of one hydroxylated metabolite of methylone (i.e., methylenedioxyamphetaminone), whose CID product ion spectrum was dominated by only one abundant ion at  $m/z$  149.0243 ( $C_8H_5O_3^+$ ). Therefore, they proposed two possible structures for that metabolite [44], a strategy we have also opted for in the present study.

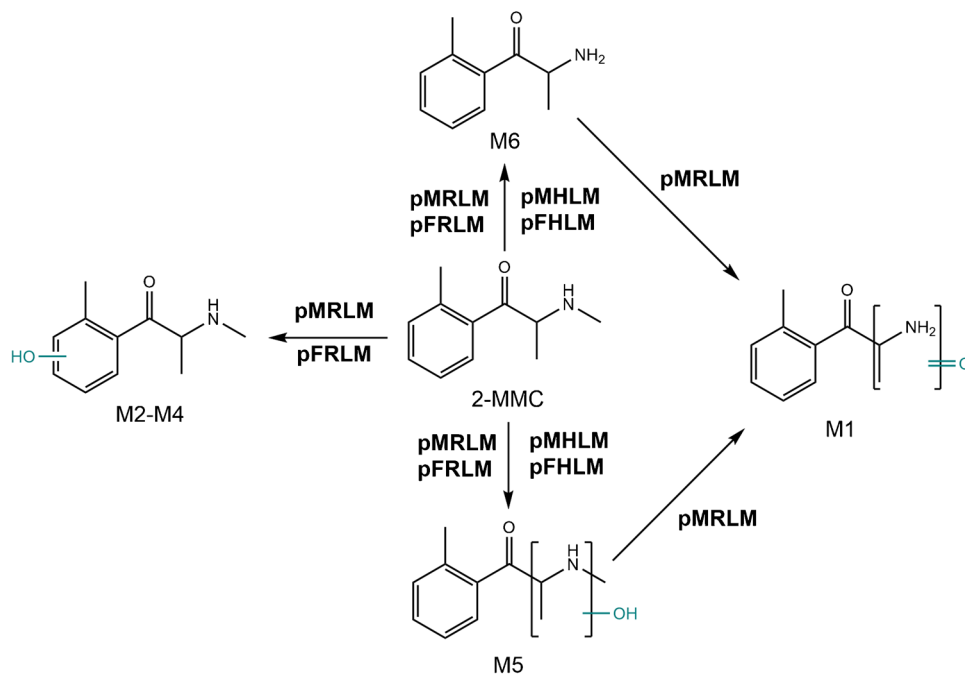
**M6** The empirical formula of this metabolite ( $C_{10}H_{14}NO^+$ ) suggests that it originates from *N*-demethylation ( $\Delta = -14$  Da). The product ion mass spectrum followed a similar fragmentation behavior as observed for the parent 2-MMC, including the dominant loss of  $H_2O$  followed by the loss of a methyl radical to form product ions at  $m/z$  146.0978 ( $C_{10}H_{12}N^+$ ) and  $m/z$  131.0742 ( $C_9H_9N^+$ ), respectively. This metabolite was detected in each of the pRLM and pHLM incubations as the most abundant metabolite observed for 2-MMC.

The *in vitro* phase I metabolic biotransformation of 2-MMC using pooled male and female rat and human liver microsomal incubations is proposed in Fig. 2.

### Identification of phase I metabolites of 3-methylmethcathinone

**M7** This metabolite was only detected in pMRLM incubations, with a protonated precursor ion detected at  $m/z$  178.0862 ( $C_{10}H_{12}NO_2^+$ ). **M7** and **M1** share the same modifications through a combination of three metabolic reactions, i.e., *N*-demethylation, *N*-oxidation, or omega-oxidation at the C-3' position, followed by dehydrogenation. The MS/MS product ion mass spectrum of this metabolite (see Fig. S1) was similar to the MS/MS product ion mass spectrum of **M1**, including the presence of diagnostic iminium ions detected at  $m/z$  86.0237 ( $C_3H_4NO_2^+$ ) and  $m/z$  58.0301 ( $C_2H_4NO^+$ ) and supporting information about the location of substitution through product ions at  $m/z$  142.0649 ( $C_{10}H_8N^+$ ),  $m/z$  119.0490 ( $C_8H_7O^+$ ), and  $m/z$  91.0540 ( $C_7H_7^+$ ). The structure of **M7** was therefore elucidated following the same procedure as **M1**, based on the presence of the same product ions in both MS/MS product ion mass spectra. Similar to **M1**, there was evidence of co-elution due to the presence of product ions at  $m/z$  160.1120 ( $C_{11}H_{14}N^+$ ) and  $m/z$  145.0886 ( $C_{10}H_{11}N^+$ ), which could not have been formed from **M7** given the accurate mass measurements. The results from the UHPLC-MS/MS analysis revealed a lack of product ions at  $m/z$  160.1120 ( $C_{11}H_{14}N^+$ ) and  $m/z$  145.0886 ( $C_{10}H_{11}N^+$ ), which suggests that the interference co-eluted with **M7** under conventional LC separation conditions, but was

**Fig. 2** Proposed metabolic pathways of 2-MMC obtained with liver microsomal incubations. The metabolite numbers correspond to the identified metabolites listed in Table 1. Abbreviations: MMC, methylmethcathinone; pMRLM, pooled male rat liver microsomes; pFRLM, pooled female rat liver microsomes; pMHLM, pooled male human liver microsomes; pFHLM, pooled female human liver microsomes





resolved under UHPLC conditions. The extracted ion chromatogram (EIC) and MS/MS product ion mass spectrum of the metabolite **M7**, including the proposed fragmentation patterns, are included in Fig. S1.

**M8–10** These three metabolites were all detected in pRLM incubations, showing a protonated precursor ion at  $m/z$  194.1175 ( $C_{11}H_{16}NO_2^+$ ). Yet, only **M8** and **M10** were discovered from pHLM incubations. The measured accurate mass at  $m/z$  194.1175 suggests that these metabolites contain one more oxygen atom than 3-MMC ( $\Delta = 16$  Da). Since 3-MMC contains several potential hydroxylation sites, the respective MS/MS product ion mass spectra were used to propose the most likely structure for each metabolite. The MS/MS product ion mass spectrum of **M8** showed a primary  $H_2O$  loss at  $m/z$  176.1068 ( $C_{11}H_{14}NO^+$ ), followed by either a second  $H_2O$  loss to obtain a product ion detected at  $m/z$  158.0963 ( $C_{11}H_{12}N^+$ ) or the loss of formaldehyde ( $CH_2O$ ) to obtain a product ion at  $m/z$  146.0963 ( $C_{10}H_{12}N^+$ ). The structure of **M8** was therefore proposed to be 3-hydroxymethylmethcathinone (3-OH-MMC), which was also found in biosamples of 3-MMC-related cases previously reported [45, 46]. It is worth mentioning that such a hydroxylated metabolite was not detected for 2-MMC. For the less abundant **M9**, the diagnostic ion at  $m/z$  135.0435 ( $C_8H_7O_2^+$ ) and the single loss of  $H_2O$  both indicate that one oxygen atom was likely introduced to the aromatic ring. However, a product ion at  $m/z$  134.0963 ( $C_9H_{12}N^+$ ) was also detected, but its tentative structure could not be determined confidently. With UHPLC-MS/MS analysis, the resulting product ion mass spectrum of **M9** did not show any product ion at  $m/z$  134.0963, but an additional diagnostic product ion at  $m/z$  107.0499 ( $C_7H_7O^+$ ) was detected, which provided further support for the elucidation that the hydroxyl group was introduced to the aromatic ring (Fig. S2. f). **M10** was formed following a similar transformation as **M5**, i.e., with the introduction of a hydroxyl group to the aliphatic chain. Two sequential losses of  $H_2O$  were observed leading to product ions detected at  $m/z$  176.1085 ( $C_{11}H_{14}NO^+$ ) and 158.0969 ( $C_{11}H_{12}N^+$ ), suggesting the presence of a hydroxyl group in the aliphatic chain. However, the MS/MS product ion mass spectrum of **M10** is again not sufficient to determine the exact location where the oxygen was introduced in the aliphatic chain. The EIC and MS/MS product ion mass spectra of the **M8–10** metabolites, including the proposed fragmentation patterns, are shown in Fig. S2.

**M11** The empirical formula of this metabolite ( $C_{10}H_{14}NO^+$ ) suggests an *N*-demethylated metabolite ( $\Delta = -14$  Da) due to the loss of a methyl group from 3-MMC. This was also consistent with the measured accurate mass at  $m/z$  164.1070. This de-alkylated metabolite was also detected in each of the pRLM and pHLM incubations as the most abundant species of 3-MMC. The EIC and MS/MS product ion mass spectrum

of **M11**, including the proposed fragmentation pattern, are illustrated in Fig. S3. The sequential loss of  $H_2O$  and a methyl radical led to the formation of product ions at  $m/z$  146.0936 ( $C_{10}H_{12}N^+$ ) and  $m/z$  131.0728 ( $C_9H_9N^+$ ), respectively.

**M12** This metabolite was only detected in pRLM incubations, with a protonated precursor ion detected at  $m/z$  210.1124 ( $C_{11}H_{16}NO_3^+$ ). Based on its accurate mass, this metabolite was produced via addition of two oxygen atoms to 3-MMC ( $\Delta = 32$  Da). The product ion mass spectrum showed an abundant ion at  $m/z$  135.0435 ( $C_8H_7O_2^+$ ), indicating aromatic hydroxylation. There were also less abundant product ions at  $m/z$  192.1021 ( $C_{11}H_{14}NO_2^+$ ) and  $m/z$  174.0913 ( $C_{11}H_{12}NO^+$ ) formed through the sequential loss of  $H_2O$ . Secondary fragmentation from the intermediate ion at  $m/z$  192.1021 ( $C_{11}H_{14}NO_2^+$ ) revealed the loss of a methanol radical ( $^*CH_2OH$ ,  $\Delta = 31$  Da) to form a product ion at  $m/z$  161.0835 ( $C_{10}H_{11}NO^+$ ) that provided further confirmation of oxidation on the aliphatic chain, *N*-oxidation, or omega-oxidation in the C-3' position. Figure S4 shows the EIC and MS/MS product ion mass spectrum of **M12**, as well as the proposed fragmentation pattern.

**M13 and M14** These two metabolites were only detected in pRLM incubation, leading to a protonated precursor ion at  $m/z$  180.1018 ( $C_{10}H_{14}NO_2^+$ ), and the accurate mass measurements identified these metabolites as compounds with hydroxylation and de-methylation. However, **M14** was generated exclusively in pMRLM incubations. The product ion mass spectrum of **M13** showed that there was a primary  $H_2O$  loss to form the product ion at  $m/z$  162.0911 ( $C_{10}H_{12}NO^+$ ), followed by either a second  $H_2O$  loss to  $m/z$  144.0807 ( $C_{10}H_{10}N^+$ ) or the loss of formaldehyde ( $CH_2O$ ) to  $m/z$  132.0807 ( $C_9H_{10}N^+$ ), yet the product ions at  $m/z$  160.1115 ( $C_{11}H_{14}N^+$ ) and  $m/z$  145.0882 ( $C_{10}H_{11}N^+$ ) could not have originated from **M13** and, thus, must have originated by another metabolite that co-eluted and was present within the 4 Da isolation window. Nonetheless, such contradictory product ions were not detected using UHPLC-MS/MS. The structure of this metabolite was tentatively elucidated as 3-hydroxymethyl-*N*-demethyl-MMC. **M14** showed that there was a primary  $H_2O$  loss to form the product ion at  $m/z$  162.0913 ( $C_{10}H_{12}NO^+$ ), followed by either a second  $H_2O$  loss to  $m/z$  144.0808 ( $C_{10}H_{10}N^+$ ) or the loss of CO to form  $m/z$  134.0966 ( $C_9H_{12}N^+$ ), indicating the likely inclusion of a hydroxyl group to the C-3' position. The EIC and MS/MS product ion mass spectra of 3-MMC **M13** and **M14**, including the proposed fragmentation patterns, are illustrated in Fig. S5.

**M15** This metabolite was detected in pRLM incubations only. The protonated precursor ion at  $m/z$  192.1021 ( $C_{11}H_{14}NO_2^+$ ) indicates that hydroxylation and dehydrogenation occurred. The sequential loss of CO and  $H_2O$  was observed through the detection of product ions at  $m/z$

164.1069 ( $C_{10}H_{14}NO^+$ ) and  $m/z$  146.0964 ( $C_{10}H_{12}N^+$ ), respectively. The structure of this metabolite was identified as 3'-aldehyde-MMC. The EIC and MS/MS product ion mass spectrum of **M15**, including the proposed fragmentation pattern, are illustrated in Fig. S6.

**M16** This metabolite was detected in pMRLM incubations only. The protonated precursor ion at  $m/z$  166.1226 ( $C_{10}H_{16}NO^+$ ) indicates that carbonyl reduction and *N*-demethylation occurred; this metabolite was therefore elucidated as 3-methylnorephedrine. The fragmentation of this metabolite is different from the other metabolites in this study, as the reduction of carbonyl inhibited indole ring formation. Such biotransformation was not observed with 2-MMC metabolic incubations. In addition to the lack of indole ring formation, **M16** fragmentation also included the formation of a product ion at  $m/z$  131.0855 ( $C_{10}H_{11}^+$ ) formed through the loss of ammonia ( $NH_3$ ) as the secondary fragmentation of

the primary product ion at  $m/z$  148.1121 ( $C_{10}H_{14}N^+$ ) formed through the loss of  $H_2O$ . The EIC and MS/MS product ion mass spectrum of **M16**, including the proposed fragmentation pattern, are illustrated in Fig. S7.

**M17** This metabolite was only detected in pRLM incubations. The protonated precursor ion at  $m/z$  208.0968 ( $C_{11}H_{14}NO_3^+$ ) indicates that carboxylation most likely occurred. The diagnostic product ions for this elucidation are  $m/z$  190.0856 ( $C_{11}H_{12}NO_2^+$ ) formed through the loss of  $H_2O$  and the subsequent product ion at  $m/z$  146.0967 ( $C_{10}H_{12}N^+$ ) formed through the loss of  $CO_2$ , which is characteristic for an aromatic carboxylic acid. This metabolite was therefore elucidated as 4-carboxymethcathinone. The EIC and MS/MS product ion mass spectrum of **M17**, including the proposed fragmentation pattern, are illustrated in Fig. S8.

The *in vitro* phase I metabolites of 3-MMC, for the first time reported, are illustrated in Fig. 3.

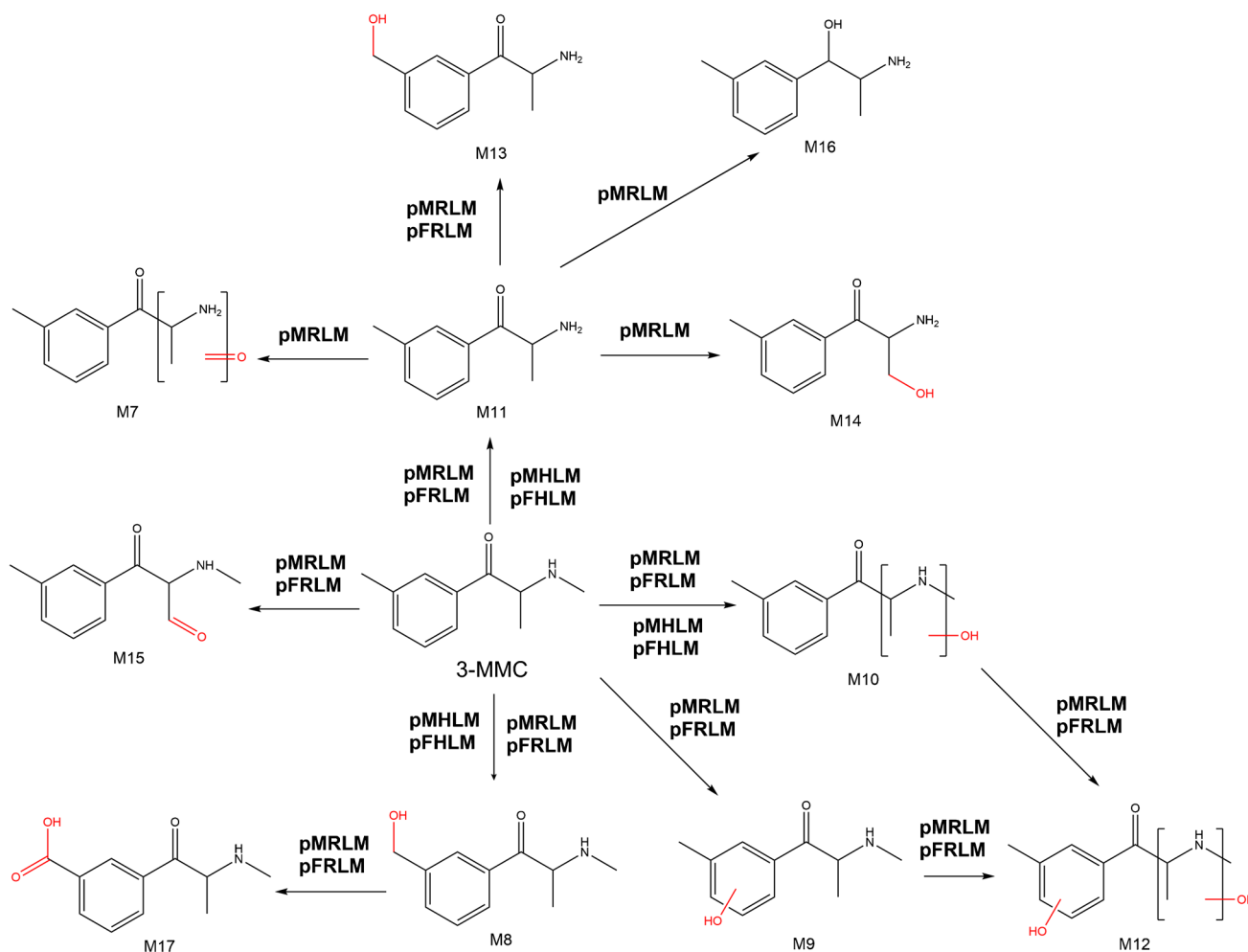


**Fig. 3** Proposed metabolic pathways of 3-MMC obtained with pooled liver microsomal incubations. The metabolite numbers correspond to the identified metabolites listed in Table 1. Abbreviations: MMC, meth-

ylmethcathinone; pMRLM, pooled male rat liver microsomes; pFRLM, pooled female rat liver microsomes; pMHLM, pooled male human liver microsomes; pFHLM, pooled female human liver microsomes

## Identification of phase I metabolites of 4-methylmethcathinone

**M18 and M19** These two metabolites were only detected in pMRLM incubations, leading to a protonated precursor ion at  $m/z$  178.0866 ( $C_{10}H_{12}NO_2^+$ ). **M19** underwent the same biotransformations as **M1** and **M7** from a combination of three metabolic reactions, which were *N*-demethylation, *N*-oxidation or omega-oxidation at the C-3' position, followed by dehydrogenation. The MS/MS product ion mass spectrum of this metabolite was similar to **M1** and **M7**, including the diagnostic ion at nominal  $m/z$  86 ( $C_3H_4NO_2^+$ ). This metabolite is reported for the first time. Compared with **M19**, **M18** is more polar, as demonstrated by a  $H_2O$  loss to the product ion at  $m/z$  160.0759 ( $C_{10}H_{10}NO^+$ ) and the loss of formaldehyde ( $CH_2O$ ) to obtain a product ion at  $m/z$  148.0759 ( $C_9H_{10}NO^+$ ). Another  $H_2O$  loss was observed from the product ion at  $m/z$  148.0759 ( $C_9H_{10}NO^+$ ), giving rise to the product ion at  $m/z$  130.0654 ( $C_9H_8N^+$ ). All these fragmentation patterns suggest that the hydroxyl was introduced to the benzyl group. The other modification to **M18** is likely due to the dehydrogenation based on the measured accurate mass of the protonated precursor ion. Nevertheless, some artifact ions were observed in the product ion mass spectrum, such as the product ion at  $m/z$  160.1125 ( $C_{11}H_{14}N^+$ ) and the one at  $m/z$  145.0890 ( $C_{10}H_{11}N^+$ ), which could not have originated from **M18**. Such contradictory product ions are likely due to co-elution, as they were not observed in the UHPLC-MS/MS product ion mass spectrum for **M18**.

**M20 and M21** These two metabolites were detected in pRLM and pHLM incubations, leading to a protonated precursor ion at  $m/z$  194.1179 ( $C_{11}H_{16}NO_2^+$ ); the accurate mass measurements indicated the presence of hydroxylation ( $\Delta = 16$  Da). **M20** had a similar fragmentation pattern as **M8**, which helped with the structural elucidation of **M20** as 4-hydroxymethylmethcathinone (4-OH-MMC). This metabolite is a primary phase I metabolite which has been identified by previous studies [18–22]. The MS/MS product ion mass spectrum of **M21** was dominated by the product ion at  $m/z$  119.0487 ( $C_8H_7O^+$ ), indicating that the aromatic moiety of 4-MMC remains intact. Previous study detected this metabolite in rat blood after oral administration and speculated that the hydroxylation was introduced to the C-3' position based on the observation of two  $H_2O$  losses and the product ion at  $m/z$  74.0591 ( $C_3H_8NO^+$ ) [22]. However, the MS/MS product ion mass spectrum of **M21** is not sufficient to determine the exact location where the oxygen atom was introduced to the aliphatic chain. A previous study also discovered an aromatic monohydroxylated metabolite from 4-MMC in vivo [22], yet this metabolite was not detected here.

**M22** The empirical formula of this metabolite ( $C_{10}H_{14}NO^+$ ) suggests the *N*-demethylated metabolite ( $\Delta = -14$  Da). This

is also consistent with the accurate mass measurement at  $m/z$  164.1073. This de-methylated metabolite was also the most abundant species of 4-MMC and was found in all in vitro metabolic incubations in this study and had been reported by previous research in the metabolism of 4-MMC [19–23].

**M23** The empirical formula of this metabolite ( $C_{11}H_{16}NO_3^+$ ) suggests a di-hydroxylation metabolite with two diagnostic ions, namely the product ion at  $m/z$  161.0828 ( $C_{10}H_{11}NO^+$ ) and the product ion at  $m/z$  135.0437 ( $C_8H_7O_2^+$ ), indicating one hydroxylation is located at the aromatic ring. This metabolite was only detected in pRLM incubations. The MS/MS product ion mass spectrum of this metabolite was similar to the MS/MS product ion mass spectrum of **M12**. The structure of **M23** was therefore elucidated following the same procedure as **M12**.

**M24** This metabolite was exclusively detected in pMRLM incubations, leading to a protonated precursor ion at  $m/z$  180.1025 ( $C_{10}H_{14}NO_2^+$ ), and the accurate mass measurement indicates this metabolite as a compound with hydroxylation and *N*-demethylation. The product ion mass spectrum showed the sequential loss of  $H_2O$  to the product ions at  $m/z$  162.0916 ( $C_{10}H_{12}NO^+$ ) and  $m/z$  144.0811 ( $C_{10}H_{10}N^+$ ), as observed previously for **M14**. The combination of these observations and the relatively longer retention time suggests that the hydroxylation probably occurred at the C-3' position.

**M25** This metabolite was only detected in pMRLM incubations. The protonated precursor ion at  $m/z$  166.1230 ( $C_{10}H_{16}NO^+$ ) indicates that reduction of the carbonyl group and *N*-demethylation occurred. The fragmentation pattern of this metabolite is the same as **M16**; therefore, **M25** was identified as 4-methylnorephedrine. This metabolite was also discovered by previous studies [20, 23, 24]. However, such biotransformation was only observed in pMRLM incubations of 4-MMC.

The metabolic pathway of 4-MMC is proposed in Fig. 4. Some phase I metabolites of 4-MMC deciphered in this study, such as **M20**, **M22**, and **M25**, are in accordance with metabolites reported in previous studies [20–24].

Overall, a total of 25 phase I metabolites of MMC positional isomers were detected and identified using pHLM and pRLM incubations. The accurate mass measurement for each metabolite enabled the determination of only one feasible elemental formula at the selected mass window ( $\pm 5$  mDa). Among the metabolites detected, six phase I metabolites were detected from 2-MMC, eleven phase I metabolites from 3-MMC, and eight phase I metabolites from 4-MMC in vitro metabolic models, respectively. Some phase I metabolites from the MMC positional isomers were also positional isomers to each other, such as **M8** and **M20**, thus sharing very similar fragmentation patterns with each other

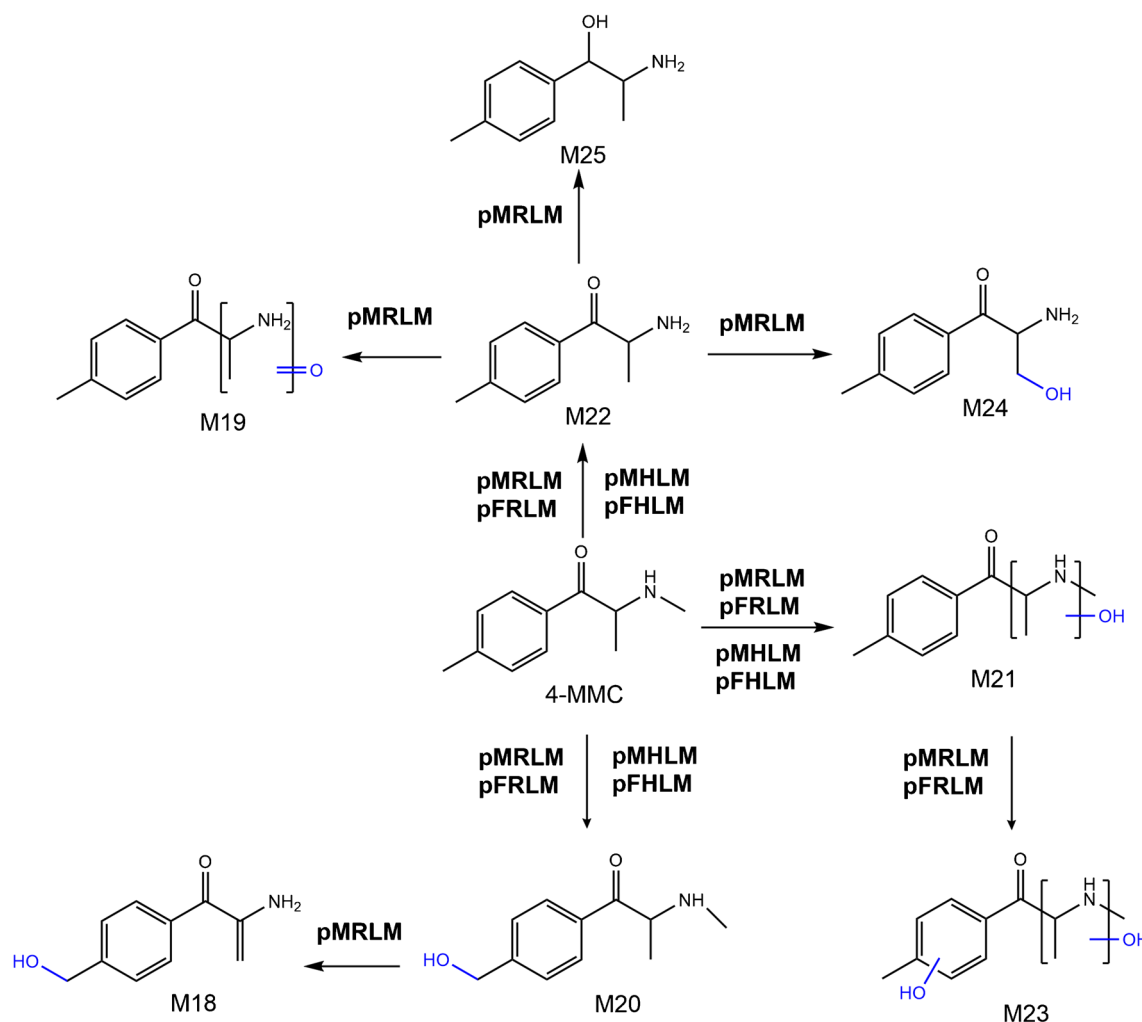


**Fig. 4** Proposed metabolic pathways of 4-MMC obtained with liver microsomal incubations. The metabolite numbers correspond to the identified metabolites listed in Table 1. Abbreviations: MMC, methyl-

methcathinone; pMRLM, pooled male rat liver microsomes; pFRLM, pooled female rat liver microsomes; pMHLM, pooled male human liver microsomes; pFHLM, pooled female human liver microsomes

as their parent compounds do. Notably, for some metabolites, such as **M1**, **M5**, **M7**, **M10**, **M12**, **M19**, **M21**, and **M23**, two possible structures were proposed for each, as their MS/MS product ion mass spectra were not sufficient to confidently determine a unique structure. Since the *in vitro* metabolism of 3-MMC using pRLM incubations is the most extensive of these metabolic incubations, the fragmentation patterns of 3-MMC metabolites are detailed in Supplementary Fig. S1–S8. A summary of all the phase I metabolites of the MMC positional isomers formed using liver microsomal incubations is shown in Table 1. Seventeen phase I metabolites were detected in pRLM incubations only, and not in pHLM incubations. Furthermore, eight metabolites were detected in both pRLM and pHLM incubations. There were a total of 25 metabolites detected in pRLM incubations; among those, seven metabolites were observed with pMRLM incubations only but not in pFRLM incubations.

### Phase I metabolism of methylmethcathinone positional isomers: general trends

*N*-Demethylation occurred for the three MMC positional isomers via the enzymatic removal of a methyl group from the nitrogen atom, resulting in the most abundant metabolites detected, namely, **M6** (from 2-MMC), **M11** (from 3-MMC), and **M22** (from 4-MMC). Also, different hydroxylated metabolites were observed in pHLM and pRLM incubations for the MMC positional isomers. For instance, the oxidation of the methyl group at the aromatic ring was observed for both 3-MMC and 4-MMC, resulting in the formation of **M8** and **M20**, respectively, but not for 2-MMC with its methyl group in the *ortho*-position, as illustrated in Fig. 5. These two metabolites, 3-OH-MMC (**M8**) and 4-OH-MMC (**M20**), are interesting as they can be used as specific biomarkers for discriminating between the consumption of 3-MMC and 4-MMC. Indeed, the

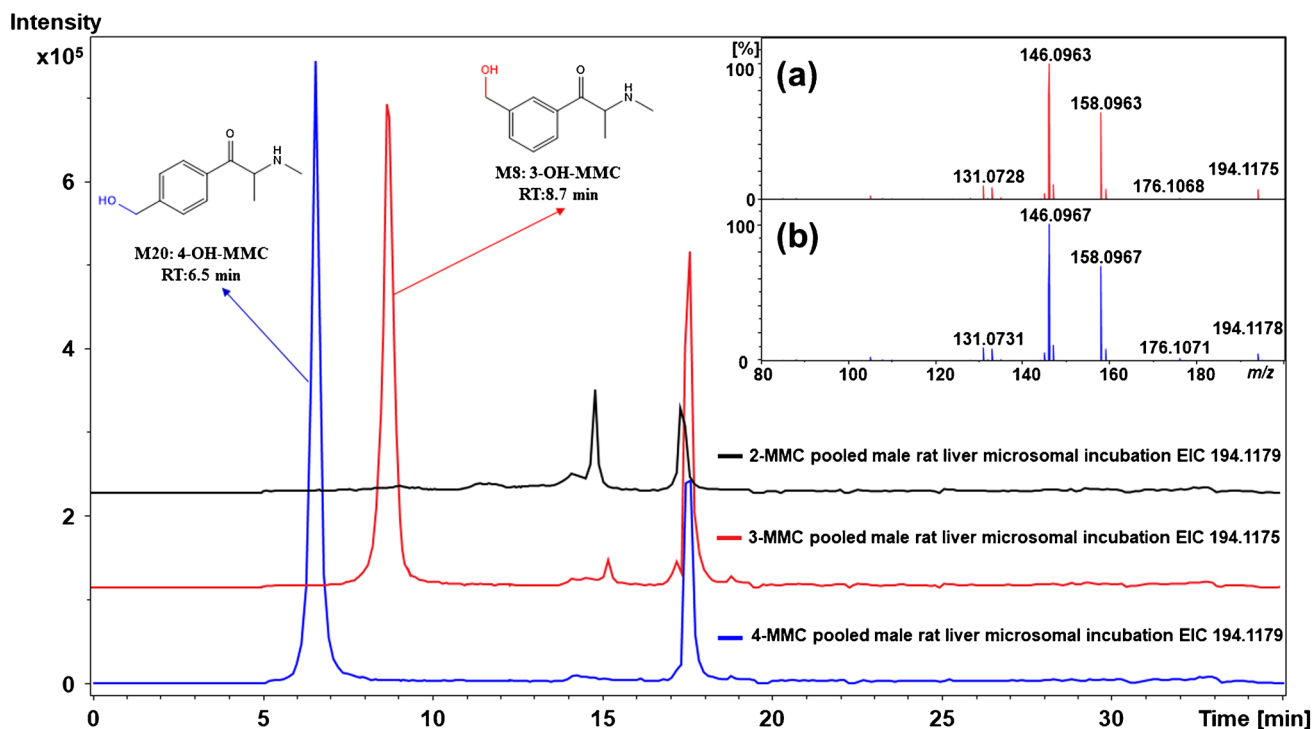


**Fig. 5** Extracted ion chromatograms (EICs) obtained for mono-hydroxylated metabolites in pooled male rat liver microsomal incubations. **(a)** Product ion mass spectrum observed for 3-OH-MMC. **(b)** Product ion mass spectrum observed for 4-OH-MMC. The metabolite

numbers correspond to the identified metabolites listed in Table 1. The retention times observed for 3-OH-MMC (8.7 min) and 4-OH-MMC (6.5 min) were significantly different. No hydroxylated metabolite was observed for 2-MMC

metabolites **M8** and **M20** eluted at 6.5 min and 8.7 min for 4-OH-MMC and 3-OH-MMC, respectively, showing a sufficient resolution to enable a clear discrimination, while their parent compounds 3-MMC and 4-MMC are often difficult to separate and distinguish from each other using conventional analytical methods [16, 47]. The analysis of such hydroxylated metabolites in body fluids may help with the identification of 3-MMC consumption and avoid the possible underestimation of the real number of cases of 3-MMC use and, in turn, its toxicity. In addition to the difference in the formation of mono-hydroxylated metabolites, the dehydrogenated metabolites were also only detected for 3-MMC and 4-MMC, namely, **M16** and **M25**.

Besides the difference in aliphatic hydroxylated metabolites observed in this study, aromatic hydroxylation metabolites were only detected for 2-MMC and 3-MMC. Additionally, di-hydroxylated metabolites (**M12** and **M23**) were observed for the metabolism of 3-MMC and 4-MMC, but not for 2-MMC.

### Differences in biotransformation of methylmethcathinone positional isomers in pooled rat liver microsomes vs. pooled human liver microsomes

The biotransformation of MMC positional isomers showed significant differences in pHLM and pRLM incubations,

where more metabolites were detected with pRLM incubations compared to pHLM incubations, as illustrated in Fig. 6. All the metabolites which were detected in pHLM incubations, i.e., **M5**, **M6**, **M8**, **M10**, **M11**, **M17**, **M18**, and **M19**, were the same as those observed with pRLM incubations (Table 1). These metabolites were derived from oxidative biotransformation via either hydroxylation or *N*-demethylation, resulting in an array of primary phase I metabolites without secondary modifications. Strikingly, secondary metabolites, such as **M12** and **M13**, arising from combinations of microsomal oxidation reactions, were observed with pRLM incubations only (Fig. 6b). Moreover, metabolites arising from aromatic hydroxylation were only detected in pRLM incubations.

Previous in vitro studies have demonstrated that CYP2D6 is the main enzyme responsible for the metabolism of 4-MMC, along with minor contributions from other drug-metabolizing enzymes, such as CYP1A2, CYP2C19, CYP2C9, and CYP3A4 [21]. The pHLM material used contained a pool of microsomes all derived from Caucasians ( $n = 10$  for each sex), which may explain why fewer metabolites were detected, as European Caucasians show a much lower level of CYP2D6 activity compared with other ethnicities due to genetic polymorphism [48]. About 7% of Caucasians are devoid of CYP2D6 activity, as they show

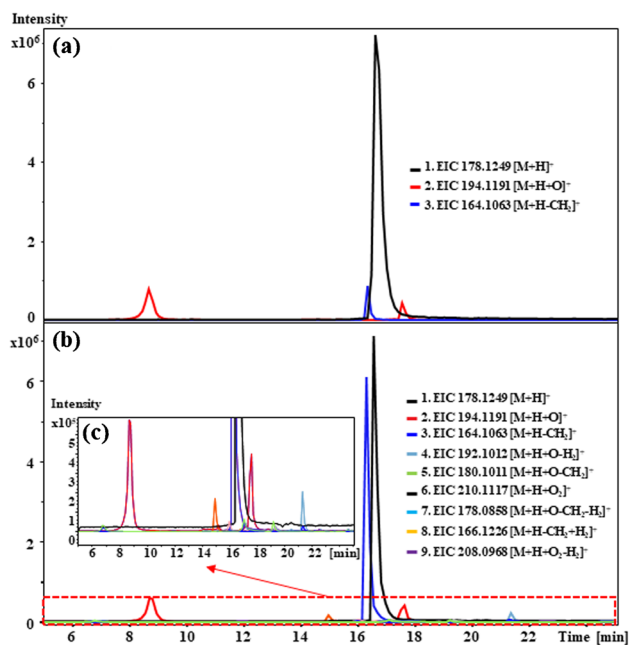
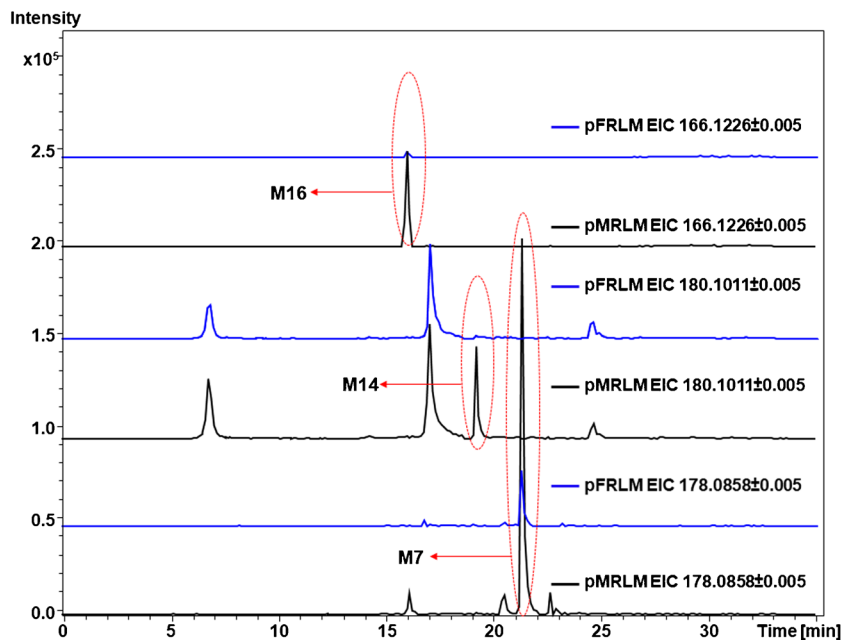


**Fig. 6** Comparisons of the extracted ion chromatograms (EICs) obtained for the metabolites of 3-MMC in pooled male human liver microsomal (pMHLM) and pooled male rat liver microsomal (pMRLM) incubations. (a) EICs of 3-MMC, **M8**, **M10**, and **M11**, which were observed in pMHLM incubations. (b) EICs of 3-MMC and **M7**–**M17**, which were generated from pMRLM incubations. (c) EICs of the less abundant metabolites generated from pMRLM incubations

two inactive CYP2D6 alleles and, thus, do not synthesize the active enzyme. The expression of cytochrome P450s and other drug-metabolizing enzymes in human is probably not

**Fig. 7** Comparisons of extracted ion chromatograms (EICs) of the discriminative metabolites **M7**, **M14**, and **M16** of 3-MMC measured in pooled male rat liver microsomal (pMRLM) incubations (black EIC traces) which were not detected in pooled female rat liver microsomal (pFRLM) incubations (blue EIC traces). The metabolite numbers correspond to the identified metabolites listed in Table 1



influenced by sex as much as in rats [49]. The pRLM in vitro metabolic incubations of each sex have sex-specific enzymes (i.e., CYP2A2, CYP2C11, CYP2C13, and CYP3A2) which are male-specific enzymes in sexually mature male rats, and CYP2C12 is a sex-specific enzyme in female rats, which consequently may have led to the formation of sex-specific metabolites.

### Sex-specific metabolism of methylmethcathinone positional isomers

The analysis of the possible sex-specific differences in the metabolism of MMC positional isomers using liver microsomal incubations showed relevant differences. Notably, more metabolites were observed in pMRLM compared with pFRLM incubations, as illustrated in Fig. 7. Indeed, seven metabolites of MMCs, all secondary metabolites (Table 1), were exclusively detected in pMRLM incubations, namely, **M1**, **M7**, **M14**, **M16**, and **M21**. The metabolites **M1**, **M7**, and **M16** underwent the same modifications as their respective parent compound, namely, *N*-demethylation and hydroxylation followed by dehydrogenation. In addition, the metabolites **M14** and **M21** were also further metabolized via the same pathway, i.e., *N*-demethylation and hydroxylation. The EICs of **M7** and **M14** observed for both sexes are shown in Fig. 6. Supplementary Fig. S9 shows the EICs of additional metabolites that were different between pMRLM and pFRLM incubations.

Sex-specific differences in oxidative metabolism of some illicit drugs, such as  $\Delta^9$ -tetrahydrocannabinol ( $\Delta^9$ -THC) from marijuana [36], MDMA [50], and (+)-methamphetamine [51], were previously reported as well. The

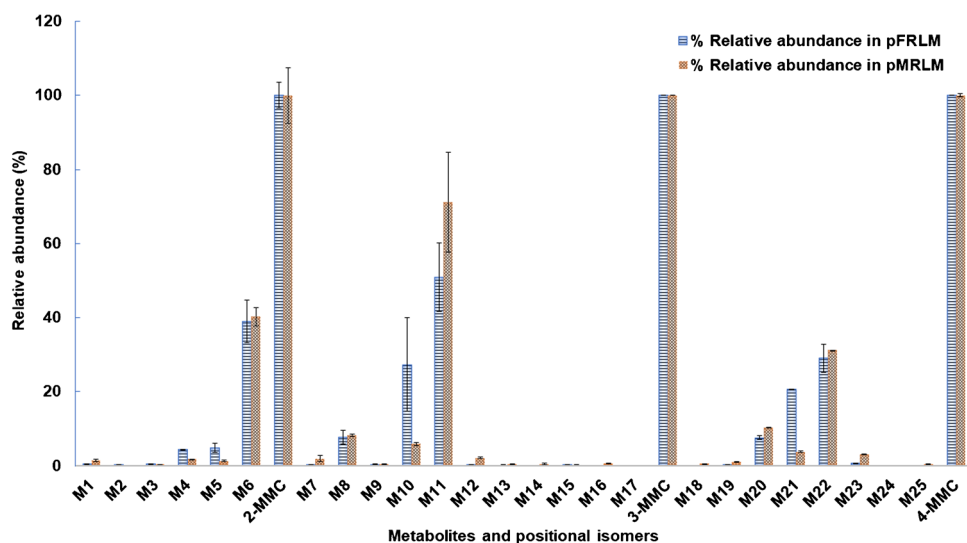


**Fig. 8** Comparison of the relative abundance observed for the tentatively identified metabolites of MMCs between pFRLM (light blue bars with lined pattern) and pMRLM (orange bars with crossed pattern) incubations. The relative abundance (%) is expressed as the average of the peak area of each metabolite or parent compound ( $n=2$ ) divided by the average of the peak areas measured for the parent compound in negative con-

trols ( $n=2$ ) and multiplied by 100. The metabolite numbers correspond to the identified metabolites listed in Table 1. The original data used for this figure are shown in Table S3. Error bars represent the relative standard deviation of the peak area ( $n=2$ ). Abbreviations: pFRLM, pooled female rat liver microsomal incubations; pMRLM, pooled male rat liver microsomal incubations; MMC, methylmethcathinone

sex differences in metabolism of  $\Delta^9$ -THC were attributed to the different forms of P450s in liver microsomes of male and female rats.  $\Delta^9$ -THC in female rats is metabolized into the active and potent metabolite 11-hydroxy- $\Delta^9$ -THC dominantly by CYP2C6, yet male rats tend to bio-transform  $\Delta^9$ -THC into multiple metabolites via CYP2C11 rather than 11-hydroxy- $\Delta^9$ -THC [36]. In vitro study of MDMA and methylenedioxyamphetamine (MDA) metabolism showed that MDMA was biotransformed into MDA more rapidly in male rat liver microsomes than female rat liver microsomes [49]. Additionally, sex- and dose-dependent differences in (+)-methamphetamine pharmacokinetics and metabolism were also observed in male and female Sprague-Dawley rats [51]. Sex-specific differences in metabolism of xenobiotics are also of significant importance from a toxicological standpoint, as the difference may produce a lower clearance of the compound, thus leading to a prolonged half-life, higher blood concentration of the parent compound, and, in turn, increased toxicity.

Besides the differences in the metabolites observed (i.e., some metabolites were observed only in pMRLM incubations), sex-specific differences in relative abundance were also observed between pFRLM incubations and pMRLM incubations (see Table S3 and Fig. 8). The phase I positional isomers primary metabolites **M5**, **M10**, and **M21** were present at a relatively higher abundance in pFRLM incubations compared with pMRLM incubations, which underwent the same modifications from their respective parent compound.

The phase I primary metabolites can be further metabolized into phase I secondary metabolites, where there were many differences observed between pFRLM incubations and pMRLM incubations. Besides forming a greater number of metabolites compared with pFRLM incubations, pMRLM incubations produced more relatively abundant secondary metabolites via further hydroxylation, demethylation, or hydroxylation with corresponding dehydrogenation. Among these metabolites, the di-hydroxylated metabolites **M12** and **M23** were observed at a relatively higher abundance in pMRLM incubations than pFRLM incubations. Finally, the *N*-demethylated metabolites (**M6**, **M11**, and **M22**) were detected at a relatively similar abundance in both sexes. Since SCs undergo metabolism via a limited number of enzymes, they might compete with each other as substrates for the same enzymes, resulting in metabolic drug-drug interactions [52]. Thus, those sex-specific differences in phase I secondary metabolism might be related with the abundance and genres of enzymes in pMRLM incubations and pFRLM incubations, where the primary metabolites were transformed into secondary metabolites more rapidly in pMRLM incubations than in pFRLM incubations. Certain CYP isozymes responsible for causing the sex-specific differences in the in vitro metabolism of NPS should be further investigated.

This study focused on the metabolic fates of the positional isomers of MMC and investigated possible sex-specific differences in their phase I metabolism. Moreover, because several isoenzymes are involved in drug metabolism

and drug-metabolizing enzymes in pFRLM and pMRLM are different in relative abundance and quality, it is essential to investigate to what extent each of these isozymes is involved in drug metabolism, especially for the sex-specific enzymes in rats, such as CYP2A2, CYP2C11, CYP2C13, and CYP3A2, in male rats and the CYP2C12 in female rats.

Strikingly, such differences in metabolite formation and their relative abundance were not observed in pMHLM versus pFHLM incubations (Supplementary Fig. S10 and Supplementary Table S4). As mentioned, the Caucasian-derived liver microsomes used in this study might partially explain this observation. Moreover, the influence of specific isozymes should be studied using liver microsomes with the addition of specific inhibitors in future research to demonstrate exactly which sex-specific isozyme(s) influence the metabolism of MMCs.

## Conclusions and perspectives

This study aimed at identifying the metabolites of MMCs using *in vitro* metabolic incubations and investigate potential sex-specific differences in MMCs biotransformation. For the first time, the biotransformation of 3-MMC and 2-MMC in liver microsomes was tentatively proposed. The consistent loss of H<sub>2</sub>O followed by the loss of a methyl radical was observed for all MMC positional isomers. Due to the oxo-function at C-1', MMC positional isomers form a conjugated indole system to maintain stability, thus resulting in the subsequent loss of radicals. This rearrangement and the favourability for the loss of H<sub>2</sub>O for *N*-alkylated synthetic cathinones explain why the product ions of most metabolites preserved the nitrogen atom. The use of isotopic labelling or MS<sup>n</sup> experiments would help future understanding of the metabolism of MMC positional isomers. In general, the metabolism of 3-MMC showed a more similar *in vitro* metabolic pattern with 4-MMC than with 2-MMC in pRLM incubations. In addition, 4-OH-MMC and 3-OH-MMC may be used as specific metabolites due to their discriminative retention time, thereby determining the consumption of the MMC positional isomer by detecting 4-OH-MMC and 3-OH-MMC, in addition to the parent compounds.

This study demonstrates that MMCs undergo a similar *in vitro* metabolic pathway in both rat and human liver microsomes, and that *N*-demethylation appears to be the main route of metabolism in *in vitro* metabolic incubations. However, the metabolism of MMCs is also dependent on the sex of the *in vitro* models. Seven metabolites were exclusively discovered in pMRLM incubations, yet this sex-specific difference was not observed in pHLM incubations. In addition, several metabolites were present in different relative abundance between the pMRLM and pFRLM incubations. These results emphasize the need to investigate the

biotransformation of xenobiotics by taking sex into consideration to have an integrated overview of their metabolism, and, thus, further improve future NPS risk assessment.

**Supplementary Information** The online version contains supplementary material available at <https://doi.org/10.1007/s00216-023-04815-3>.

**Acknowledgements** Peng Che is funded by a China Scholarship Council (CSC) fellowship (No. 202006210045). Ruben Kranenburg (Amsterdam Dutch Police, The Netherlands) is kindly acknowledged for providing the analytical standards of MMCs. Filip Cuyckens (Janssen R&D, Belgium) and Wilfried Niessen (hyphen MassSpec, the Netherlands) are warmly acknowledged for assisting in MS/MS data interpretation.

## Declarations

**Conflict of interest** The authors declare no competing interests.

**Open Access** This article is licensed under a Creative Commons Attribution 4.0 International License, which permits use, sharing, adaptation, distribution and reproduction in any medium or format, as long as you give appropriate credit to the original author(s) and the source, provide a link to the Creative Commons licence, and indicate if changes were made. The images or other third party material in this article are included in the article's Creative Commons licence, unless indicated otherwise in a credit line to the material. If material is not included in the article's Creative Commons licence and your intended use is not permitted by statutory regulation or exceeds the permitted use, you will need to obtain permission directly from the copyright holder. To view a copy of this licence, visit <http://creativecommons.org/licenses/by/4.0/>.

## References

- Schifano F, Papanti GD, Orsolini L, Corkery JM. Novel psychoactive substances: the pharmacology of stimulants and hallucinogens. *Expert Rev Clin Pharmacol*. 2016;9(7):943–54. <https://doi.org/10.1586/17512433.2016.1167597>.
- Meyer MR. New psychoactive substances: an overview on recent publications on their toxicodynamics and toxicokinetics. *Arch Toxicol*. 2016;90(10):2421–44. <https://doi.org/10.1007/s00204-016-1812-x>.
- Peacock A, Bruno R, Gisev N, Degenhardt L, Hall W, Sedefov R, White J, Thomas KV, Farrell M, Griffiths P. New psychoactive substances: challenges for drug surveillance, control, and public health responses. *Lancet*. 2019;394(10209):1668–84. [https://doi.org/10.1016/S0140-6736\(19\)32231-7](https://doi.org/10.1016/S0140-6736(19)32231-7).
- Niello M, Cintulova D, Raithmayr P, Holy M, Jantsch K, Colas C, Ecker GF, Sitte HH, Mihovilovic MD. Effects of hydroxylated mephedrone metabolites on monoamine transporter activity *in vitro*. *Front Pharmacol*. 2021;12:654061. <https://doi.org/10.3389/fphar.2021.654061>.
- Coppola M, Mondola R. Synthetic cathinones: chemistry, pharmacology and toxicology of a new class of designer drugs of abuse marketed as “bath salts” or “plant food.” *Toxicol Lett*. 2012;211(2):144–9. <https://doi.org/10.1016/j.toxlet.2012.03.009>.
- Valente MJ, Guedes de Pinho P, de Lourdes BM, Carvalho F, Carvalho M. Khat and synthetic cathinones: a review. *Arch Toxicol*. 2014;88(1):15–45. <https://doi.org/10.1007/s00204-013-1163-9>.
- European Monitoring Centre for Drugs and Drug Addiction (2022), New psychoactivesubstances: 25 years of early warning



- and response in Europe. An update from the EU Early Warning System (June 2022), Publications Office of the European Union, Luxembourg. <https://doi.org/10.2810/88231810.2810/396103>.
8. European Monitoring Centre for Drugs and Drug Addiction (2022), European Drug Report 2022: Trends and Developments, Publications Office of the European Union, Luxembourg. [https://www.emcdda.europa.eu/publications/edr/trends-developments/2022\\_en](https://www.emcdda.europa.eu/publications/edr/trends-developments/2022_en)
  9. Prosser JM, Nelson LS. The toxicology of bath salts: a review of synthetic cathinones. *J Med Toxicol.* 2012;8(1):33–42. <https://doi.org/10.1007/s13181-011-0193-z>.
  10. Cozzi NV, Sievert MK, Shulglin AT, Jacob P 3rd, Ruoho AE. Inhibition of plasma membrane monoamine transporters by beta-ketoamphetamines. *Eur J Pharmacol.* 1999;381(1):63–9. [https://doi.org/10.1016/s0014-2999\(99\)00538-5](https://doi.org/10.1016/s0014-2999(99)00538-5).
  11. Kehr J, Ichinose F, Yoshitake S, Goiny M, Sievertsson T, Nyberg F, Yoshitake T. Mephedrone, compared with MDMA (ecstasy) and amphetamine, rapidly increases both dopamine and 5-HT levels in nucleus accumbens of awake rats. *Br J Pharmacol.* 2011;164(8):1949–58. <https://doi.org/10.1111/j.1476-5381.2011.01499.x>.
  12. European Monitoring Centre for Drugs and Drug Addiction (2022), Risk assessment report on the new psychoactive substance 2-(methylamino)-1-(3-methylphenyl)propan-1-one (3-methylmethcathinone, 3-MMC) in accordance with Article 5c of Regulation (EC) No 1920/2006 (as amended), Risk Assessments, Publications Office of the European Union, Luxembourg. [https://www.emcdda.europa.eu/publications/risk-assessments/3-mmc\\_en](https://www.emcdda.europa.eu/publications/risk-assessments/3-mmc_en)
  13. Nugteren-van Lonkhuyzen JJ, Essink S, Rietjens SJ, Ohana D, de Lange DW, van Riel AJHP, Hondebrink L. 3-Methylmethcathinone (3-MMC) poisonings: acute clinical toxicity and time trend between 2013 and 2021 in the Netherlands. *Ann Emerg Med.* 2022; 80(3):203–12. <https://doi.org/10.1016/j.annemergmed.2022.04.022>.
  14. Zawilska JB. Mephedrone and other cathinones. *Curr Opin Psychiatry.* 2014;27(4):256–62. <https://doi.org/10.1097/YCO.000000000000066>.
  15. Sedefov R. Report on the risk assessment of BZP in the framework of the Council decision on new psychoactive substances. vol 8. Office for Official Publications of the European Communities; 2009.
  16. Backberg M, Lindeman E, Beck O, Helander A. Characteristics of analytically confirmed 3-MMC-related intoxications from the Swedish STRIDA project. *Clin Toxicol (Phila).* 2015;53(1):46–53. <https://doi.org/10.3109/15563650.2014.981823>.
  17. Ferreira B, Dias da Silva D, Carvalho F, de Lourdes BM, Carmo H. The novel psychoactive substance 3-methylmethcathinone (3-MMC or metaphedrone): a review. *Forensic Sci Int.* 2019;295:54–63. <https://doi.org/10.1016/j.forsciint.2018.11.024>.
  18. Olesti E, Farre M, Papaseit E, Krotonoulas A, Pujadas M, de la Torre R, Pozo OJ. Pharmacokinetics of mephedrone and its metabolites in human by LC-MS/MS. *AAPS J.* 2017;19(6):1767–78. <https://doi.org/10.1208/s12248-017-0132-2>.
  19. Czerwinska J, Jang M, Costa C, Parkin MC, George C, Kicman AT, Bailey MJ, Dargan PI, Abbate V. Detection of mephedrone and its metabolites in fingerprints from a controlled human administration study by liquid chromatography-tandem mass spectrometry and paper spray-mass spectrometry. *Analyst.* 2020;145(8):3038–48. <https://doi.org/10.1039/c9an02477h>.
  20. Pozo OJ, Ibanez M, Sancho JV, Lahoz-Beneytez J, Farre M, Papaseit E, de la Torre R, Hernandez F. Mass spectrometric evaluation of mephedrone *in vivo* human metabolism: identification of phase I and phase II metabolites, including a novel succinyl conjugate. *Drug Metab Dispos.* 2015;43(2):248–57. <https://doi.org/10.1124/dmd.114.061416>.
  21. Pedersen AJ, Reitzel LA, Johansen SS, Linnet K. *In vitro* metabolism studies on mephedrone and analysis of forensic cases. *Drug Test Anal.* 2013;5(6):430–8. <https://doi.org/10.1002/dta.1369>.
  22. Martinez-Clemente J, Lopez-Arnau R, Carbo M, Pubill D, Camarasa J, Escubedo E. Mephedrone pharmacokinetics after intravenous and oral administration in rats: relation to pharmacodynamics. *Psychopharmacology.* 2013;229(2):295–306. <https://doi.org/10.1007/s00213-013-3108-7>.
  23. Linhart I, Himl M, Zidkova M, Balikova M, Lhotkova E, Palenicek T. Metabolic profile of mephedrone: Identification of normephedrone conjugates with dicarboxylic acids as a new type of xenobiotic phase II metabolites. *Toxicol Lett.* 2016;240(1):114–21. <https://doi.org/10.1016/j.toxlet.2015.10.025>.
  24. Khreit OI, Grant MH, Zhang T, Henderson C, Watson DG, Sutcliffe OB. Elucidation of the Phase I and Phase II metabolic pathways of (+/-)-4'-methylmethcathinone (4-MMC) and (+/-)-4'-(trifluoromethyl)methcathinone (4-TFMMC) in rat liver hepatocytes using LC-MS and LC-MS(2). *J Pharm Biomed Anal.* 2013;72:177–85. <https://doi.org/10.1016/j.jpba.2012.08.015>.
  25. Gavrilović I, Gelu Y, Abbate V. *In Vitro* metabolic study of four synthetic cathinones: 4-MPD, 2-NMC, 4F-PHP and bk-EPDP. *Metabolites.* 2022;12(2):115–34. <https://doi.org/10.3390/metabo12020115>.
  26. Lopes BT, Caldeira MJ, Gaspar H, Antunes AMM. Metabolic Profile of Four Selected Cathinones in Microsome Incubations: Identification of Phase I and II Metabolites by Liquid Chromatography High Resolution Mass Spectrometry. *Front Chem.* 2020;8:609251. <https://doi.org/10.3389/fchem.2020.609251>.
  27. Nykodemova J, Sulakova A, Palivec P, Ceskova H, Rimpelova S, Sichova K, Leonhardt T, Jurasek B, Hajkova K, Palenicek T, Kuchar M. 2C-B-Fly-NBOMe metabolites in rat urine, human liver microsomes and *C. elegans*: confirmation with synthesized analytical standards. *Metabolites.* 2021;11(11):775. <https://doi.org/10.3390/metabo11110775>.
  28. Manier SK, Schwermer F, Wagmann L, Eckstein N, Meyer MR. Liquid Chromatography-High-Resolution Mass Spectrometry-Based *In Vitro* Toxicometabolomics of the Synthetic Cathinones 4-MPD and 4-MEAP in Pooled Human Liver Microsomes. *Metabolites.* 2020;11(1):3. <https://doi.org/10.3390/metabo11010003>.
  29. Di Trana A, Brunetti P, Giorgetti R, Marinelli E, Zaami S, Busardo FP, Carlier J. *In silico* prediction, LC-HRMS/MS analysis, and targeted/untargeted data-mining workflow for the profiling of phenylfentanyl *in vitro* metabolites. *Talanta.* 2021;235:122740. <https://doi.org/10.1016/j.talanta.2021.122740>.
  30. Richter LHJ, Herrmann J, Andreas A, Park YM, Wagmann L, Flockerzi V, Muller R, Meyer MR. Tools for studying the metabolism of new psychoactive substances for toxicological screening purposes - a comparative study using pooled human liver S9, HepaRG cells, and zebrafish larvae. *Toxicol Lett.* 2019;305:73–80. <https://doi.org/10.1016/j.toxlet.2019.01.010>.
  31. Soldin OP, Mattison DR. Sex differences in pharmacokinetics and pharmacodynamics. *Clin Pharmacokinet.* 2009;48(3):143–57. <https://doi.org/10.2165/00003088-200948030-00001>.
  32. Bigos KL, Pollock BG, Stankevich BA, Bies RR. Sex differences in the pharmacokinetics and pharmacodynamics of antidepressants: an updated review. *Gend Med.* 2009;6(4):522–43. <https://doi.org/10.1016/j.genm.2009.12.004>.
  33. Farkouh A, Riedl T, Gottardi R, Czejka M, Kautzky-Willer A. Sex-related differences in pharmacokinetics and pharmacodynamics of frequently prescribed drugs: a review of the literature. *Adv Ther.* 2020;37(2):644–55. <https://doi.org/10.1007/s12325-019-01201-3>.
  34. Fattore L, Marti M, Mostallino R, Castelli MP. Sex and Gender Differences in the Effects of Novel Psychoactive Substances.

- Brain Sci. 2020;10(9):606. <https://doi.org/10.3390/brainsci10090606>.
35. Tseng AH, Harding JW, Craft RM. Pharmacokinetic factors in sex differences in Delta 9-tetrahydrocannabinol-induced behavioral effects in rats. *Behav Brain Res.* 2004;154(1):77–83. <https://doi.org/10.1016/j.bbr.2004.01.029>.
  36. Narimatsu S, Watanabe K, Yamamoto I, Yoshimura H. Sex difference in the oxidative metabolism of delta 9-tetrahydrocannabinol in the rat. *Biochem Pharmacol.* 1991;41(8):1187–94. [https://doi.org/10.1016/0006-2952\(91\)90657-q](https://doi.org/10.1016/0006-2952(91)90657-q).
  37. Mugford CA, Kedderis GL. Sex-dependent metabolism of xenobiotics. *Drug Metab Rev.* 1998;30(3):441–98. <https://doi.org/10.3109/03602539808996322>.
  38. Kool J, Ramautar R, van Liempd SM, Beckman J, de Kanter FJ, Meerman JH, Schenk T, Irth H, Commandeur JN, Vermeulen NP. Rapid on-line profiling of estrogen receptor binding metabolites of tamoxifen. *J Med Chem.* 2006;49(11):3287–92. <https://doi.org/10.1021/jm0507936>.
  39. Davidson JT, Sasiene ZJ, Jackson GP. Fragmentation pathways of odd- and even-electron N-alkylated synthetic cathinones. *Int J Mass Spectrom.* 2020;453:ARTN 116354. <https://doi.org/10.1016/j.ijms.2020.116354>.
  40. Zuba D. Identification of cathinones and other active components of 'legal highs' by mass spectrometric methods. *Trac-Trend Anal Chem.* 2012;32:15–30. <https://doi.org/10.1016/j.trac.2011.09.009>.
  41. Davidson JT, Sasiene ZJ, Abiedalla Y, DeRuiter J, Clark CR, Jackson GP. Fragmentation pathways of alpha-pyrrolidinophenone synthetic cathinones and their application to the identification of emerging synthetic cathinone derivatives. *Int J Mass Spectrom.* 2020;453:ARTN 116343. <https://doi.org/10.1016/j.ijms.2020.116343>.
  42. Fornal E. Study of collision-induced dissociation of electrospray-generated protonated cathinones. *Drug Test Anal.* 2014;6(7–8):705–15. <https://doi.org/10.1002/dta.1573>.
  43. Tyler Davidson J, Piacentino EL, Sasiene ZJ, Abiedalla Y, DeRuiter J, Clark CR, Berden G, Oomens J, Ryzhov V, Jackson GP. Identification of novel fragmentation pathways and fragment ion structures in the tandem mass spectra of protonated synthetic cathinones. *Forensic Chem.* 2020;19:100245. <https://doi.org/10.1016/j.forc.2020.100245>.
  44. Pedersen AJ, Petersen TH, Linnet K. In vitro metabolism and pharmacokinetic studies on methylone. *Drug Metab Dispos.* 2013;41(6):1247–55. <https://doi.org/10.1124/dmd.112.050880>.
  45. Aknouche F, Ameline A, Gheddar L, Maruejols C, Kintz P. Fatal rectal injection of 3-MMC in a sexual context. Toxicological investigations including metabolites identification using LC-HRMS. *J Anal Toxicol.* 2022;46(8):949–55. <https://doi.org/10.1093/jat/bkac048>.
  46. Frison G, Frasson S, Zancanaro F, Tedeschi G, Zamengo L. Detection of 3-methylmethcathinone and its metabolites 3-methylphenedrine and 3-methylnorephedrine in pubic hair samples by liquid chromatography-high resolution/high accuracy Orbitrap mass spectrometry. *Forensic Sci Int.* 2016;265:131–7. <https://doi.org/10.1016/j.forsciint.2016.01.039>.
  47. Burch HJ, Clarke EJ, Hubbard AM, Scott-Ham M. Concentrations of drugs determined in blood samples collected from suspected drugged drivers in England and Wales. *J Forensic Leg Med.* 2013;20(4):278–89. <https://doi.org/10.1016/j.jflm.2012.10.005>.
  48. Mizutani T. PM frequencies of major CYPs in Asians and Caucasians. *Drug Metab Rev.* 2003;35(2–3):99–106. <https://doi.org/10.1081/dmr-120023681>.
  49. Parkinson A, Mudra DR, Johnson C, Dwyer A, Carroll KM. The effects of gender, age, ethnicity, and liver cirrhosis on cytochrome P450 enzyme activity in human liver microsomes and inducibility in cultured human hepatocytes. *Toxicol Appl Pharmacol.* 2004;199(3):193–209. <https://doi.org/10.1016/j.taap.2004.01.010>.
  50. Fonsart J, Menet MC, Declèves X, Galons H, Crete D, Debray M, Scherrmann JM, Noble F. Sprague-Dawley rats display metabolism-mediated sex differences in the acute toxicity of 3,4-methylenedioxyamphetamine (MDMA, Ecstasy). *Toxicol Lett.* 2008;180:S159–S159. <https://doi.org/10.1016/j.toxlet.2008.06.310>.
  51. Milesi-Halle A, Hendrickson HP, Laurenzana EM, Gentry WB, Owens SM. Sex- and dose-dependency in the pharmacokinetics and pharmacodynamics of (+)-methamphetamine and its metabolite (+)-amphetamine in rats. *Toxicol Appl Pharmacol.* 2005;209(3):203–13. <https://doi.org/10.1016/j.taap.2005.04.007>.
  52. Tyrkko E, Andersson M, Kronstrand R. The toxicology of new psychoactive substances: synthetic cathinones and phenylethylamines. *Ther Drug Monit.* 2016;38(2):190–216. <https://doi.org/10.1097/FTD.0000000000000263>.

**Publisher's note** Springer Nature remains neutral with regard to jurisdictional claims in published maps and institutional affiliations.